Table XIII. Comparison of Sensitivities $\partial \ln V_j/\partial \ln V^e(\alpha\text{-oxalic acid})$ and $\partial \ln V_j/\partial \ln V^e(\beta\text{-oxalic acid})$ for the Carboxylic Acid Crystals Evaluated at the Experimental Configuration[a]

carboxylic acid	form of oxalic acid	
	α	β
acetic acid	0.48	0.67
adipic acid	0.43	0.65
α-oxalic acid	1.0	0.89
β-oxalic acid	0.92	1.0
butaric acid	0.34	0.54
formic acid	0.73	1.0
glutaric acid	0.44	0.69
malonic acid	0.57	0.80
methylmalonic acid	0.38	0.69
propionic acid	0.34	0.61
valeric acid	0.32	0.52

[a] V_j and V^e are the calculated lattice energy for the jth carboxylic acid crystal and the experimental lattice energy for the α and β crystalline form of oxalic acid.

manner the coefficients uncover relationships that are not intuitively apparent.

Conclusion

Until recently, the primary focus of the increased interest in molecular mechanics and dynamics has been toward its application and not toward the underpinnings of the generation of more accurate potential energy functions. Now, with more appreciation of the importance of the latter issue, activity in this area has developed, along with a need to approach it in a systematic manner. In this paper we have reported on the application of sensitivity analysis to the derivation of intermolecular parameters from experimental crystal data. These coefficients have proven to be valuable in elucidating the relationship between the optimized potential function and the observables used in the fitting procedure. The first class of sensitivities studied was that of the elemental sensitivities $\partial O_i/\partial \ln \alpha_j$, which proved to be useful in determining the relative importance of a parameter in defining the value of a specific observable. This information is useful for probing where changes in the potential can be made, to reduce the residual sum of squares. As an example of the former, they could be used to locate interactions that are pivotal to the binding of a substrate to an enzyme. This would be done by calculating the parametric sensitivities of important distances defining the enzyme–substrate complex and then identifying the largest sensitivities associated with these distances. In addition, when the observables are torques and forces, the coefficients specify which parameters are important in causing structural shifts away from a given conformation. This feature is also important for understanding structure–function and structure–property issues. In addition to using the elemental sensitivities to analyze the relationship between the observable and potential parameters, the derived coefficients were also shown to be valuable for understanding their relationship. These quantities are used to directly probe the questions of which observables are necessary to determine a specific parameter and what new experiments would be useful to augment the available set.

The present paper has not attempted to close the loop on potential improvement by implementing the suggestions revealed by the sensitivities. Rather, the purpose of this paper was to illustrate the type and quality of information available from performing a sensitivity analysis. The loop will be closed in a following paper.

Acknowledgment. The support of this work by the National Institutes of Health is gratefully acknowledged. In addition, one of the authors (H.R.) would like to acknowledge partial support for this research from the Squibb Institute for Medical Research and the Office of Naval Research.

Intrazeolite Carbonyl(η^5-cyclopentadienyl)dihydridoiridium(III) ($CpIr(CO)H_2$–$M_{56}Y$, Where M = H, Li, Na, K, Rb, and Cs)

Linda Crowfoot, Geoffrey A. Ozin,* and Saim Özkar†

Contribution from Lash Miller Chemistry Laboratories, University of Toronto, 80 Saint George Street, Toronto, Ontario, Canada M5S 1A1. *Received June 4, 1990*

Abstract: Vapor-phase impregnation and thermal equilibration of $CpIr(CO)H_2$ in dehydrated $M_{56}Y$ (where M = H, Li, Na, K, Rb, and Cs) yields samples in which the guest displays two main anchoring modes. In $Li_{56}Y$ and $Na_{56}Y$, a $CpIrH_2(CO)\cdots M^+$ interaction is favored (type I), whereas in $K_{56}Y$, $Rb_{56}Y$, and $Cs_{56}Y$ the preferred-binding geometry involves $CpIr(CO)H_2\cdots M^+$ (type II). The topology, spacial requirements, and ionic potential of the site II M^+ cations appear to be mutually responsible for "lock-and-key" anchoring effects of $CpIr(CO)H_2$ in the supercage of zeolite Y. The thermal and photochemical reactivities of $CpIr(CO)H_2$–$M_{56}Y$ toward D_2, HBr, CO, C_6H_6, and alkanes are investigated and compared with the situation known in solution. With D_2, one finds only H/D exchange of the hydride ligands to yield intrazeolite $CpIr(CO)D_2$–$M_{56}Y$ without hydride or Cp ring hydrogen scrambling, while exposure to CO yields the known intrazeolite species $CpIr(CO)_2$–$M_{56}Y$. In the case of both Brønsted acid $H_{56}Y$ and proton-loaded $(HBr)_8$–$Na_{56}Y$ zeolites, one discovers a proton-induced, reductive-elimination, dimerization reaction, which yields the novel intrazeolite dimer $Cp_2Ir_2(CO)_2$–$M_{56}Y$ anchored to a supercage Brønsted acid site via one of its bridge carbonyl ligands. By contrast to the situation found in solution, $CpIr(CO)H_2$–$M_{56}Y$ so far appears to be photochemically and thermally inactive toward C–H bond activation chemistry with arenes and alkanes.

Introduction

Species of the type $CpIrLH_2$ (where L = CO and PR_3) have evoked much interest in solution-phase organometallic chemistry and homogeneous catalysis mainly because of their ability to participate in reactions of the type illustrated in Scheme I.[1,2] In 1982, Janowicz and Bergman discovered that photolysis of $Cp^*Ir(PMe_3)H_2$ in the presence of alkanes yields the C–H bond inserted product $Cp^*Ir(PMe_3)(R)H$.[3] After the reported synthesis

† On leave of absence from the Chemistry Department, Middle East Technical University, Ankara, Turkey.

(1) Spousler, M. B.; Weiller, B. H.; Stoutland, P. O.; Bergman, R. G. *J. Am. Chem. Soc.* **1989**, *111*, 6841 and references cited therein.

(2) Heinekey, D. M.; Millar, J. M.; Koetzle, T. F.; Payne, N. G.; Zilm, K. W. *J. Am. Chem. Soc.* **1990**, *112*, 909 and references cited therein.

0002-7863/91/1513-2033$02.50/0

Scheme I

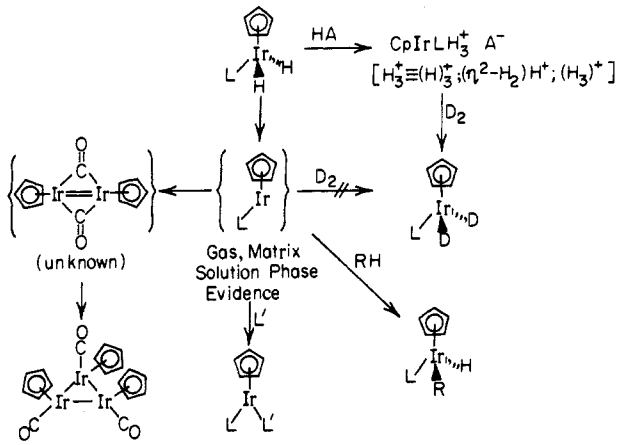

of CpIr(CO)H_2 by Shapley and Adair[4] in 1982, Graham, Rest, and co-workers[5] demonstrated its ability to photoinsert into the C–H bond of saturated hydrocarbons in solution at room temperature and even in matrices at 12 K. The matrix-isolation studies indicated that, with CH_4, the reactive 16e coordinately unsaturated CpIr(CO) intermediate was involved in the insertion reaction with a diagnostic IR peak at 1954 cm^{-1}. Shaply and Adair[3] concluded from their studies that many of the solution-phase reactions of CpIr(CO)H_2 also proceeded via the same intermediate. Deuterium-labeling techniques originally indicated that this same intermediate was involved in the solution-phase exchange of D_2.[3] More recent solution-phase work has indicated that this D_2-exchange reaction is actually caused by acid and that D_2 incorporation proceeds dissociatively via the cationic trihydride species.[2] Decarbonylation products included the trimer $Cp_3Ir_3(CO)_3$, which was also presumed to form via CpIr(CO).[3] Ligand-substitution reactions were postulated to be dissociative with respect to dihydrogen to produce compounds of the type CpIr(CO)L (for L = PPh_3, $PPhMe_2$, CO, and *t*-BuNC).[6] Recently Heinekey and Payne[7] have proposed that a trihydrogen species CpIr(L)$(H_3)^+$ forms from the protonation of CpIr(L)H_2 by HBF_4·Et_2O (when L = PMe_3, PPh_3, and $AsPh_3$).

It is interesting to note that although the CpIr(L)H_2 species have been under active investigation in the solution, gas, and matrix phases, its anchoring chemistry and reactivity on catalyst supports, such as oxides, polymers, and zeolites, have not previously been reported. Because of our earlier interest in intrazeolite organometallics like $(\eta^5\text{-}C_5H_5)M(CO)_2$ (M = Co, Rh, Ir),[8] $(\eta^5\text{-}C_5H_5)_2M$ (M = Cr, Fe, Co),[9] $M(CO)_6$ (M = Cr, Mo, W),[10] $Co_2(CO)_8$,[11] and $(\eta^6\text{-}C_6H_6)_2M$ (M = Ti, V, Cr)[12] and the important and fascinating chemistry outlined above for $CpIrLH_2$ (Scheme I), we decided to undertake a comprehensive study of CpIr(CO)H_2 in $M_{56}Y$ (where M = H, Li, Na, K, Rb, and Cs). One can consider that the potential advantages of incorporating CpIr(CO)H_2 in a zeolite Y large-pore framework material include the following: (a) the opportunity to anchor a known alkane-activating organometallic moiety inside a molecule size- and shape-discriminating support, (b) the chance of stabilizing highly reactive, coordinately unsaturated 16e species like CpIr(CO), and (c) the possibility of enhancing the chemical and catalytic activity of the precursor CpIr(CO)H_2 or reactive intermediates like CpIr(CO) through interactions with framework oxygens or extraframework cations. The latter phenomenon was recently realized for the first time with ^{13}CO isotope-exchange reactions of CpIr(CO)$_2$–$M_{56}Y$[8a] and CpCo(CO)$_2$–$M_{56}Y$[8b] and more recently with ^{12}CO substitution reactions of Mo(CO)$_6$–$M_{56}Y$ with ^{13}Co and PMe_3.[8c] The following is an account of our studies of the novel intrazeolite system CpIr(CO)H_2–$M_{56}Y$.

Experimental Section

Materials. The high-purity, crystalline sodium zeolite Y with the unit-cell composition $Na_{56}(AlO_2)_{56}(SiO_2)_{136}$·$xH_2O$ was obtained from Dr. Edith Flanigen at Union Carbide, Tarrytown, NY. To remove cation defect sites, thermally dehydrated/calcined $Na_{56}Y$ was slurried with 0.01 M NaCl/0.01 M NaOH solution and washed until free of Cl^-. Other alkali-metal zeolites $M_{56}Y$ (where M = Li, K, Rb, and Cs) as well as $(NH_4)_{56}Y$ and $H_{56}Y$ were prepared by the use of standard ion-exchange techniques and deamination procedures.[13] Far-IR spectra of the alkali-metal zeolites used indicated essentially complete ion exchange.[14] All zeolite samples were stored over saturated NH_4Cl solution to ensure a constant humidity until use. CpIr(CO)$_2$[15] and CpIr(CO)Br_2[16] were synthesized according to literature procedures. For the synthesis of CpIr(CO)H_2, essentially the same procedure as described earlier[3,6] was used. In contrast to the earlier description, CpIr(CO)H_2 is found not to be stable at room temperature, even in pentane solution. The volatile CpIr(CO)H_2 was vaporized at temperatures below 0 °C from a highly concentrated pentane solution directly into the vacuum thermally dehydrated zeolite Y wafer. CpIr(^{13}CO)H_2 was prepared in the same way from CpIr(^{13}CO)$_2$, which was synthesized by photochemical exchange of ^{13}CO and CpIr(CO)$_2$ in pentane. Anhydrous research grade hydrogen bromide, deuterium, and carbon-13-labeled carbon monoxide were purchased from Matheson and used without any further purification.

Spectroscopic Cells and Equipment. The work reported in this paper used specially designed cells for complete in situ treatments. The combined mid-IR transmission/UV–visible reflectance cell basically consists of a Pyrex tube with NaCl infrared windows at one end joined via a metal O-ring-sealed flange to a dehydration quartz tube at the other end.[17] Thermal treatments in the quartz-tube section of the cell can be carried out up to temperatures of about 500 °C. The zeolite wafers are supported in a stainless steel holder, which can easily be moved into place between the NaCl or quartz windows to obtain a mid-IR transmission or UV–visible reflectance spectrum at any point of the experiment. Two greaseless stopcocks allow for the organometallic sample to be attached at one side of the cell and for a vacuum to be applied at the other during organometallic vapor-phase impregnation of the zeolite wafer. Alternatively, the cell can be attached to a gas line for the introduction of reactants such as D_2 or CO.

The combined mid/far-IR cell was designed to study the wafer before and after in situ treatment with organometallics with use of both the mid- and far-IR probe.[11] The cell basically consists of a quartz tube with NaCl windows at one end (mid-IR part) joined to a stainless steel section with polyethylene windows at the other end (far-IR part) via a stainless steel flange. A stainless steel wafer holder can be moved easily from the dehydration zone to either the mid- or far-IR part of the cell to record the respective spectra of the same sample at each stage of the study. Two greaseless stopcocks allow for the organometallic sample to be attached at one side of the cell and for a vacuum to be applied at the other during organometallic vapor-phase impregnation of the zeolite wafer.

Spectrometers. The mid-IR spectra were obtained on a Nicolet 20SXB FTIR spectrometer. All spectra presented have been obtained by subtraction of the initial spectrum of the dehydrated zeolite from that of the organometallic-impregnated sample, followed by base-line cor-

(3) Janowicz, A. H.; Bergman, R. G. *J. Am. Chem. Soc.* **1982**, *104*, 352; **1983**, *105*, 3929.
(4) Shapley, J. R.; Adair, P. C.; Lawson, R. J.; Pierpont, C. G. *Inorg. Chem.* **1982**, *21*, 1702.
(5) Bloyce, P. E.; Rest, A. J.; Whitwell, I.; Graham, W. A. G.; Holmes-Smith, R. J. *Chem. Soc., Chem. Commun.* **1988**, 846.
(6) Adair, P. C. Dissertation, University of Illinois, Urbana, IL, 1980.
(7) Heinekey, D. M.; Payne, N. G.; Schulte, G. K. *J. Am. Chem. Soc.* **1988**, *110*, 2303.
(8) (a) Ozin, G. A.; Haddleton, D. M.; Gil, C. J. *J. Phys. Chem.* **1989**, *93*, 6710. (b) Li, X.; Ozin, G. A.; Özkar, S. *J. Phys. Chem.*, in press. Ozin, G. A.; Pastore, H. O., Özkar, S.; Poe, A. J.; Vichi, E. J. S. *J. Chem. Soc., Chem. Commun.*, in press.
(9) Ozin, G. A.; Godber, J. P. *J. Phys. Chem.* **1989**, *93*, 878.
(10) Özkar, S.; Ozin, G. A.; Bein, T.; Moeller, K. *J. Am. Chem. Soc.* **1990**, *112*, 9575.
(11) Ozin, G. A.; Baker, M. D.; Godber, J. P.; Gil, C. J. *J. Phys. Chem.* **1989**, *93*, 2899.
(12) Ozin, G. A.; Godber, J. P. Intrazeolite Organometallics: Chemical and Spectroscopic Probes of Internal Versus External Confinement of Metal Guests. *The Chemistry of Excited States and Reactive Intermediates*; Lever, A. P. B., Ed.; ACS Symposium Series 307; American Chemical Society: Washington, DC, 1986.
(13) Dwyer, J.; Dyer, A. *Chem. Ind.* **1984**, *237*; see also references cited therein.
(14) Ozin, G. A.; Godber, J. G.; Baker, M. D. *Catal. Rev.-Sci. Eng.* **1985**, *27*, 591.
(15) Rausch, M. D.; Andrews, P. S.; Gardner, S. A. *Inorg. Chem.* **1973**, *12*, 2396.
(16) King, R. B. *Inorg. Chem.* **1966**, *5*, 82.
(17) Ozin, G. A.; Godber, J. G. *J. Phys. Chem.* **1988**, *92*, 4980.

rection. Far-IR spectra were obtained on a Nicolet 20F FTIR spectrometer. Optical reflectance spectra were obtained on a Perkin-Elmer 330 spectrometer with a $BaSO_4$ disk as reference. Powder X-ray diffraction (XRD) patterns were recorded on a Phillips PW 1051 diffractometer with Ni-filtered Cu Kα radiation (1.541 78 Å).

Experimental Procedure. About 20 mg of size-sieved zeolite crystals was pressed into a self-supporting wafer with a diameter of 16 mm by applying a pressure of 5 tons/in.^{2} for 10 s. The disks were secured in the stainless steel sample holder and placed in the quartz part of the cell. The thermal dehydration of the wafer under dynamic vacuum, with an Omega Series CN-2010 programmable temperature controller, followed a preset temperature schedule: 25–100 °C over 1 h, 1 h at 100 °C, 100–450 °C over 3 h, and 1 h at 450 °C. This was followed by calcination in a static atmosphere of 300 Torr of oxygen at 450°C for 1 h and pumping hot at this temperature. The degree of dehydration was judged by the flatness of the base line in the IR ν_{OH} stretching and δ_{OH} deformation regions of 3400–3700 and 1600–1650 cm^{-1}, respectively. When a sufficiently dehydrated sample was obtained, the wafer was moved into place above the organometallic sample holder. When the stopcock to the sample holder was opened, exposure to the organometallic vapor under dynamic vacuum was continued until an absorbance of 1–2 units was obtained in the carbonyl mid-IR region corresponding to a loading of about 0.3–0.4 $CpIr(CO)H_2$ molecules/α-cage. Reaction time varied from 3 to 5 min, with $CpIr(CO)H_2$/pentane held at 0 °C. Further evacuation was carried out under dynamic vacuum at room temperature in order to remove the residual pentane adsorbed on the zeolite wafer during the vapor-phase impregnation of the organometallic.

Calculated ν_{CO} frequencies and C–O bond stretching/interaction force constants for various metal carbonyl moieties were obtained with the programs of McIntosh and Peterson[18] togcther with use of the Cotton–Kraihanzel force field approximation.[19]

Elemental analyses for Na, Al, and Ir were performed by neutron activation analysis on the University of Toronto Slow Poke Reactor.

Molecular Modeling. CHEM-X software, produced and sold by Chemical Design Ltd., Oxford, England, and run on a VAX 8650 computer, was employed to perform some informative molecular modeling on various alkali-metal zeolite Y α-cage-encapsulated $CpIr(CO)H_2$ and $Cp_2Ir_2(CO)_2$ moieties. The basic zeolite Y host lattice bond lengths and angles were taken from the reported crystal structure.[20] Initial structural parameters for α-cage-located $CpIr(CO)H_2$ and $Cp_2Ir_2(CO)_2$ species were estimated from the known crystal structures of similar compounds.[1,21,22,28]

Results and Discussion

Solvent and support effects involving $CpIr(CO)H_2$ can be probed in an especially revealing way by vibrational spectroscopy because of the sensitivity of distinct ν_{CH}, ν_{IrH}, and ν_{CO} fingerprint stretching modes with respect to specific interactions involving the cyclopentadienyl, hydride, and carbonyl ligands, respectively. By example, changes in solvent from argon to methylene chloride shift the ν_{IrH} from 2189 to 2156 cm^{-1} and the ν_{CO} from 2018 to 2002 cm^{-1}. One anticipates that, by attaching $CpIr(CO)H_2$ to, for example, zeolite supports, similar perturbations of these fingerprint modes will be observed, the direction and magnitude of which will be related to the nature of the anchoring site and the strength of binding. Simultaneous observation of the far-IR adsorption induced cation translatory mode shifts will provide additional clues about the location (internal or external), homogeneity, and site of attachment of $CpIr(CO)H_2$ in the zeolite Y host.[11,23]

Intrazeolite $CpIr(CO)H_2$–$M_{56}Y$ (M = Li, Na, K, Rb, Cs)

A summary of the mid-IR spectra for the in situ impregnation of gaseous $CpIr(CO)H_2$ into vacuum thermally dehydrated $M_{56}Y$ (where M = Li, Na, K, Rb, and Cs) is shown in Figure 1. These data were collected for loading levels of less than one $CpIr(CO)H_2$/α-cage. Recall that there are eight α-cages in a unit cell of zeolite Y.[24] Saturation loading was found (from elemental analysis) to correspond to precisely two $CpIr(CO)H_2$/α-cage for the samples studied. The key features of these mid-IR spectra for $CpIr(CO)H_2$–$M_{56}Y$ are the following.

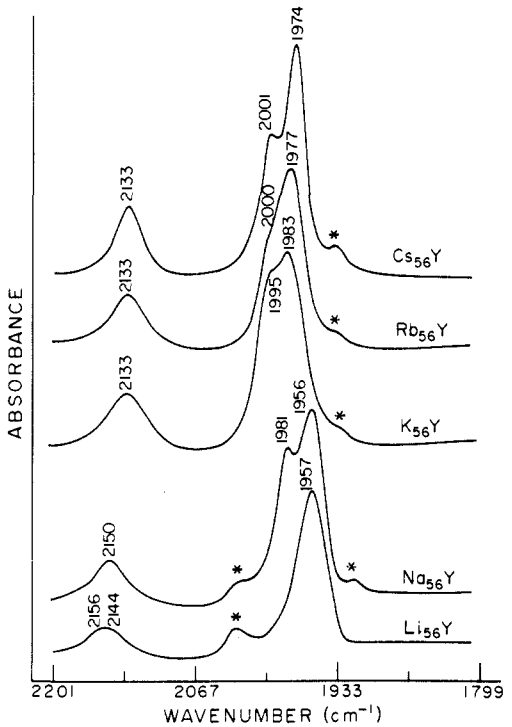

Figure 1. Representative mid-IR spectra for freshly impregnated $CpIr(CO)H_2$–$M_{56}Y$ (where M = Li, Na, K, Rb, and Cs). Loading-dependent ν_{CO} satellite bands indicated with an asterisk (see text).

(i) **Two** main regions of absorption for the ν_{CH} mode of the $Li_{56}Y/Na_{56}Y$ (3118/3112 cm^{-1}) and $K_{56}Y/Rb_{56}Y/Cs_{56}Y$ (3101/3096/3092 cm^{-1}) samples, with the average value of the latter group at **lower** frequencies.

(ii) **Two** main regions of absorption for the ν_{IrH} mode of the $Li_{56}Y/Na_{56}Y$ and $K_{56}Y/Rb_{56}Y/Cs_{56}Y$ samples, with the average value of the latter group at **lower** frequencies.

(iii) **Two** main regions of absorption for the ν_{CO} mode of the $Li_{56}Y/Na_{56}Y$ and $K_{56}Y/Rb_{56}Y/Cs_{56}Y$ samples, with the average value of the latter group at **higher** frequencies.

(iv) Freshly impregnated $CpIr(CO)H_2$–$M_{56}Y$, with the exception of Li^+, rather than displaying the expected ν_{CO} **singlet** in the region of 2000 cm^{-1} (as found in solution) instead appears as a major **doublet**.

Deuterium and ^{13}CO labeling (see later) has confirmed the assignment of the hydride and carbonyl bands, as well as the fact that the stoichiometry of the encapsulated species is indeed $CpIr(CO)H_2$. The main effect of increased loading on the mid-IR spectra of freshly impregnated $CpIr(CO)H_2$–$M_{56}Y$ is to cause the appearance of weak satellite bands on the main ν_{CO} modes (indicated by an asterisk in Figure 1, see later).

Site Redistribution of $CpIr(CO)H_2$–$M_{56}Y$

In all freshly impregnated $CpIr(CO)H_2$–$M_{56}Y$ samples (with the exception of Li), the intensities of the ν_{CO} components of the main doublet (Figure 1) are observed to slowly transform at room temperature to yield a picture in which only one component dominates. A representative illustration of this redistribution effect for $CpIr(CO)H_2$–$Cs_{56}Y$ is shown in Figure 2, from which it can be discerned that the higher frequency ν_{CO} component around 2000 cm^{-1} gives way to the lower one at 1974 cm^{-1}. Concurrently, minor frequency shifts of about 1–2 cm^{-1} are observed on the respective ν_{CH} and ν_{IrH} modes. A parallel situation is found to exist for M = K, Rb, and Cs. Interestingly, this effect for M = Na appears

(18) McIntosh, D. F.; Peterson, M. R. BMAT, FTRY/ATOM, FFIT; Quantum Chemistry Program Exchange, No. 342, Room 204, Indiana University: Bloomington, IN 47401.
(19) Cotton, F. A.; Kraihanzel, C. S. *J. Am. Chem. Soc.* **1962**, *84*, 4432.
(20) Fitch, A. N.; Jobic, H.; Renouprez, A. *J. Phys. Chem.* **1986**, *90*, 1311.
(21) Cirjak, L. M.; Ginsburg, R. E.; Dahl, L. F. *Inorg. Chem.* **1982**, *21*, 940.
(22) Ricci, J. S.; Koetzle, T. F.; Fernandez, M. J.; Maitlis, P. M.; Green, J. C. *J. Organomet. Chem.* **1986**, *299*, 383.
(23) Godber, J.; Baker, M. D.; Ozin, G. A. *J. Phys. Chem.* **1989**, *93*, 1409.
(24) Breck, D. W. *Zeolite Molecular Sieves*; Wiley: New York, 1974.

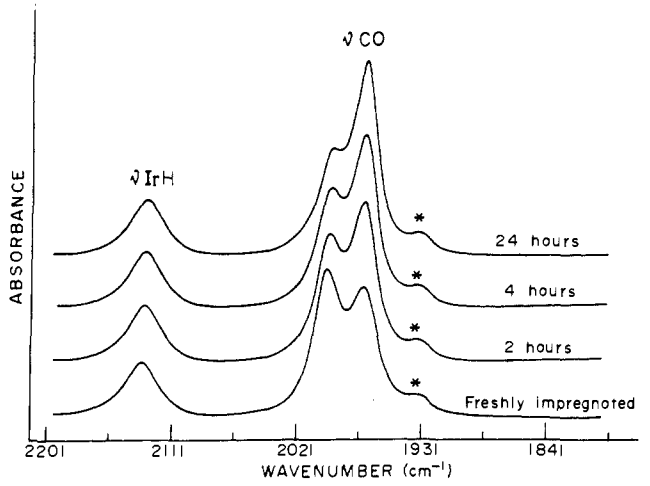

Figure 2. Room temperature "thermal annealing" effect of freshly impregnated $CpIr(CO)H_2$–$Cs_{56}Y$.

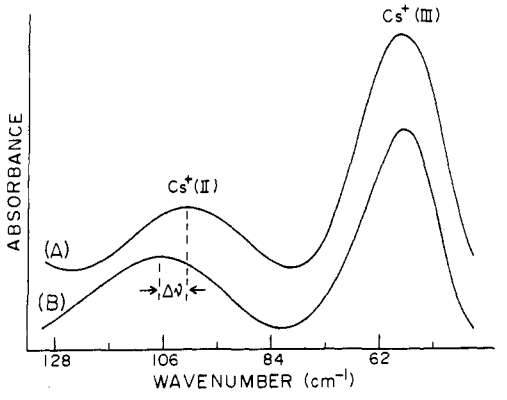

Figure 3. Far-IR spectra of (A) dehydrated $Cs_{56}Y$ and (B) $CpIr(CO)H_2$–$Cs_{56}Y$.

to depend on the loading of $CpIr(CO)H_2$. At loadings of more than one $CpIr(CO)H_2$/α-cage, the redistribution follows that described above for M = K, Rb, and Cs. At lower values, it is the higher frequency ν_{CO} component of the doublet that, at room temperature, grows in at the expense of the lower one.

Anchoring Modes and Binding Sites for $CpIr(CO)H_2$–$M_{56}Y$

The natural division of the mid-IR spectra of $CpIr(CO)H_2$–$M_{56}Y$ into what appears to be **two** distinct groups (Figure 1) associated with M = Li and Na and M = K, Rb, and Cs implies the existence of two main modes of attachment of the organometallic guest in the supercage of the zeolite Y host. The slow room temperature ν_{CO} spectral changes observed for each of these anchoring types (Figure 2) appears to be associated with a kind of "annealing" process in which a newly encapsulated $CpIr(CO)H_2$ guest spontaneously "docks" and settles down into its thermodynamically stable binding site in the supercage of zeolite Y.

The far-IR spectra of $CpIr(CO)H_2$–$M_{56}Y$ are rich in information concerning the precise binding site for the two main anchoring modes of $CpIr(CO)H_2$ in the supercage of zeolite Y. A representative set of data are portrayed in Figure 3 for $CpIr(CO)H_2$–$Cs_{56}Y$.

In the far-IR spectrum of the virgin dehydrated $Cs_{56}Y$ (Figure 3), one clearly observes two cation translatory modes around 102 and 57 cm^{-1}, signaling the presence of the expected supercage Cs^+ cations residing in sites II and III, respectively.[23] Impregnation of $CpIr(CO)H_2$ into $Cs_{56}Y$ induces a Cs^+ site II specific frequency shift from 102 to 107 cm^{-1}, leaving the Cs^+ site III absorption essentially unchanged (Figure 3). Similar results were obtained for $Na_{56}Y$ as the representative case of the second kind of anchoring mode for $CpIr(CO)H_2$ in zeolite Y. As well as pinpointing the α-cage site II cations as the binding points for the two classes of anchoring mode found for $CpIr(CO)H_2$–$M_{56}Y$, the far-IR observations provide evidence for internal confinement of the guest in the zeolite Y crystals, rather than a location on their external surface.[11]

Some more experimental clues that support the internal location and cation binding site model proposed above are presented in the following section. This will then set the stage for the construction of a topological model for the two anchoring modes types I and II unveiled for $CpIr(CO)H_2$–$M_{56}Y$ (where M = Li and Na and M = K, Rb, and Cs, respectively).

Internal versus External Confinement of $CpIr(CO)H_2$–$M_{56}Y$.

The kinetic diameter[24] of $CpIr(CO)H_2$ is estimated to be 6.1 × 6.8 Å. It is therefore expected to be size excluded from K_8Na_4A zeolite, which has an 8-ring entrance window diameter of 3 Å but permitted free access to the supercage of $Na_{56}Y$ through the 12-ring entrance window with diameter 7.8–8.0 Å. It was found that exposure of dehydrated K_8Na_4A to the vapor of $CpIr(CO)H_2$ produced an IR spectrum that was essentially "solutionlike". Room temperature evacuation of this sample caused rapid removal of the adsorbed $CpIr(CO)H_2$ species, a situation that is considered diagnostic of a physisorbed species weakly bound and confined to the external surface layers of the K_8Na_4A crystals. By sharp contrast, the same species exposed to dehydrated $Na_{56}Y$, as described earlier (Figure 1), yields an IR spectrum that shows an appreciable perturbation of all fingerprint ν_{CH}, ν_{IrH}, and ν_{CO} stretching modes attributed to a significant interaction of the $CpIr(CO)H_2$ guest with extraframework supercage cations.[25] Moreover, even though $CpIr(CO)H_2$ is an extremely volatile oil at room temperature, evacuation of $CpIr(CO)H_2$–$Na_{56}Y$ at 10^{-6} Torr and 80 °C leaves its characteristic mid-IR spectrum unchanged. Exposure of $CpIr(CO)H_2$ to all-silica Y (SiO_2–Y, the cation-free version of $Na_{56}Y$) yields a mid-IR spectrum that is essentially "solutionlike". However, unlike $CpIr(CO)H_2$–$Na_{56}Y$, when $CpIr(CO)H_2$–SiO_2–Y is exposed to a room temperature dynamic vacuum, "all trace" of the encapsulated guest is lost in seconds. Together the above observations provide compelling evidence that $CpIr(CO)H_2$–$M_{56}Y$ is internally anchored to the supercage cations via the various ligands bonded to the iridium(III) center. Evidence for different types of anchoring modes are discussed in the next section.

Topological Model for $CpIr(CO)H_2$–$M_{56}Y$ Anchoring Modes

The key points that must be encompassed by any topological model for the encapsulated $CoIr(CO)H_2$ guest in the $M_{56}Y$ (M = Li, Na, K, Rb, Cs) zeolite Y host are the following: (i) α-cage confinement, (ii) site II cation binding sites, (iii) type I anchoring mode favored in $Li_{56}Y$ and $Na_{56}Y$, (iv) type II anchoring mode favored in $K_{56}Y$, $Rb_{56}Y$, and $Cs_{56}Y$, (v) strongly perturbed CO and Cp ligands for the type I binding site, (vi) strongly perturbed hydride ligands for the type II binding site, (vii) saturation loading of two $CpIr(CO)H_2$/α-cage, and (viii) pseudo-tetrahedral coordination geometry around the Ir(III) center.

A model that can nicely accommodate all of the points listed above considers the mutual topological and spacial requirements of the tetrahedrally disposed site II extraframework cations in the α-cage with respect to the $CpIr(CO)H_2$ guest as sketched in Chart I.

The smaller site II cations Li^+ and Na^+ reside in, or close to, the plane of the α-cage six-ring sites, respectively.[26] The larger site II cations K^+, Rb^+, and Cs^+ progressively protrude further into the supercage.[26] Within the alkali-metal-cation zeolite Y series, one finds that the accessible space between adjacent site II cations monotonically diminishes on passing from Li^+ to Cs^+. CHEM-X space-filling models for $CpIr(CO)H_2$ in the α-cage environment of $M_{56}Y$ indicate that the larger Cp and CO ligands are likely to straddle between **two** of the more distant adjacent Li^+ and Na^+ cations, while the smaller hydride ligands can more comfortably bind to a **single** cation in the case of K^+, Rb^+, and

(25) Godber, J.; Ozin, G. A. *J. Phys. Chem.* **1989**, *93*, 878.
(26) Mortier, W. J. *Compilation of Extraframework Sites in Zeolites*; Butterworth: Survey, U.K., 1982.

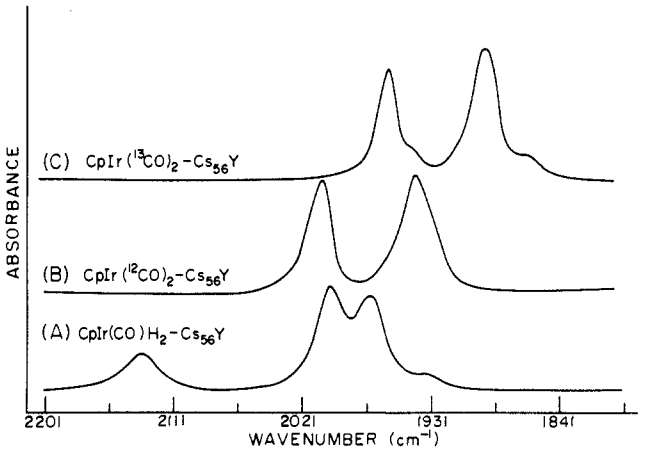

Figure 4. In situ mid-IR study of the room temperature reaction of CpIr(^{12}CO)H$_2$-Cs$_{56}$Y with ^{12}CO and ^{13}CO to yield CpIr(^{12}CO)$_2$-Cs$_{56}$Y and CpIr(^{13}CO)$_2$-Cs$_{56}$Y, respectively: (A) CpIr(^{12}CO)H$_2$-Cs$_{56}$Y, (B) CpIr(^{12}CO)$_2$-Cs$_{56}$Y, and (C) CpIr(^{13}CO)$_2$Cs$_{56}$Y.

Chart I

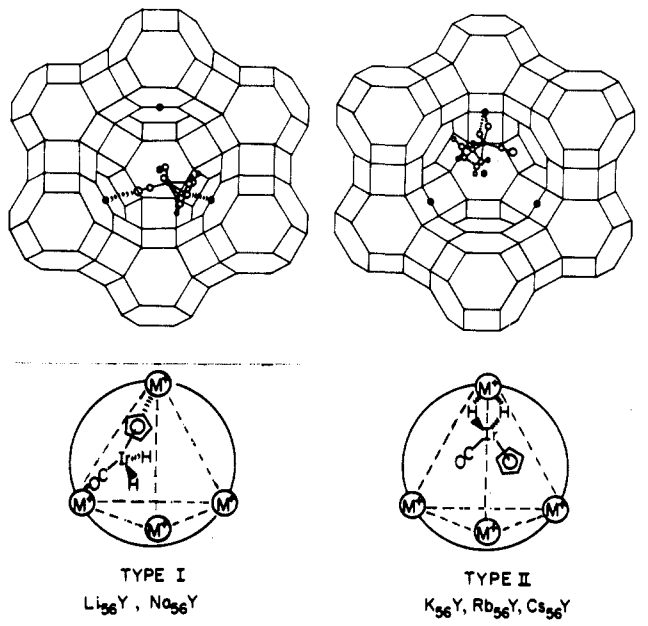

Cs^+ as illustrated in Chart I. These models are consistent with the majority of the experimental observations described above.

As mentioned earlier, weak ν_{CO} satellite lines (indicated with an asterisk in Figure 1) grow in near the main ν_{CO} bands at loading levels that favor the coexistence of two CpIr(CO)H$_2$ guests in the same α-cage. Under these circumstances, it is possible that extra vibrational modes in the ligand stretching region could arise from correlation coupling between CpIr(CO)H$_2$ partners housed within a common supercage.

Chemistry of Intrazeolite CpIr(CO)H$_2$-M$_{56}$Y

(a) Carbon Monoxide. Some of the chemical reactions of CpIr(CO)H$_2$-M$_{56}$Y are found to be much the same as those that occur in solution (Scheme I). For instance upon treatment with ^{12}CO, the CpIr(CO)H$_2$-M$_{56}$Y species spontaneously transforms into CpIr(CO)$_2$-M$_{56}$Y as found in solution (Figure 4). The mid-IR spectra of CpIr(CO)$_2$-M$_{56}$Y formed intrazeolitically in this way is identical with that found by Gil, Haddleton, and Ozin[8] on directly subliming CpIr(CO)$_2$ into M$_{56}$Y. The CpIr(CO)H$_2$-M$_{56}$Y precursor cannot be regenerated from CpIr(CO)$_2$-M$_{56}$Y upon treatment with H$_2$ either thermally or photolytically, again as found in solution. Confirmation of the ^{12}CO reaction scheme can be found from the results of the corresponding ^{13}CO experiment, the results of which are also shown in Figure 4. One observes the gradual conversion of CpIr(^{12}CO)H$_2$-M$_{56}$Y

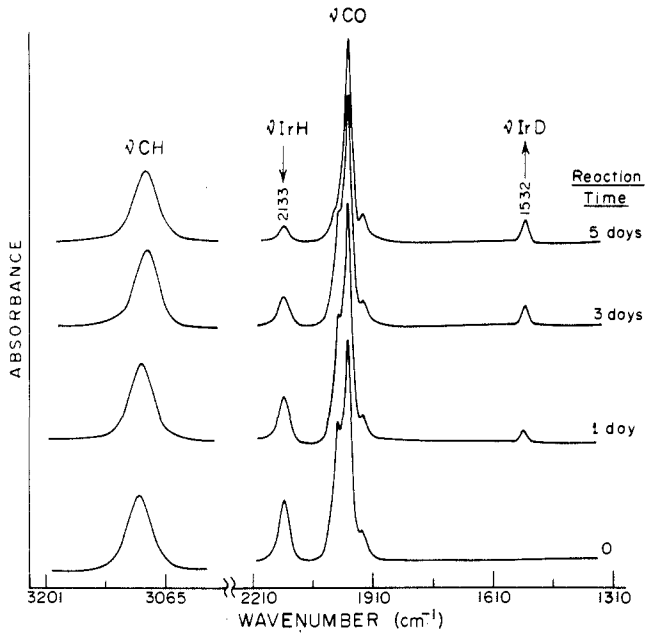

Figure 5. In situ mid-IR study of the room temperature reaction of CpIr(CO)H$_2$-Cs$_{56}$Y with D$_2$.

Scheme II

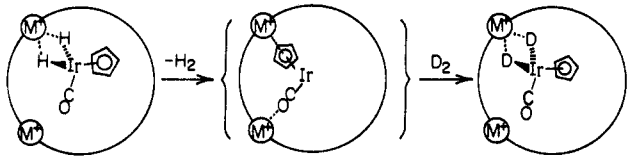

to CpIr(^{12}CO)(^{13}CO)-M$_{56}$Y and finally to CpIr(^{13}CO)$_2$-M$_{56}$Y, consistent with the facile ^{12}CO/^{13}CO isotope-exchange reactions of CpIr(^{12}CO)$_2$-M$_{56}$Y discovered by Gil, Haddleton, and Ozin.[8]

(b) Dihydrogen. The CpIr(CO)H$_2$-M$_{56}$Y type II species are found to undergo a slow H/D exchange reaction when exposed to D$_2$ gas in which no mixed isotopic species of the type CpIr(CO)HD-M$_{56}$Y are observed (Figure 5). Furthermore, the cyclopentadienyl ring hydrogens do not undergo any H/D exchange under these conditions (Figure 5). It appears that a dissociative H/D exchange reaction of the type shown in Scheme II can operate for type II CpIr(CO)H$_2$-M$_{56}$Y, although the data do not rigorously exclude nonpairwise H$_2$/D$_2$ exchange processes. As type I CpIr(CO)H$_2$-M$_{56}$Y does not appear to be active toward H/D exchange reactions of the above type, one presumes that it is the cation–cyclopentadienyl and cation–carbonyl interactions of the kind shown in Chart I that are responsible for deactivating type I CpIr(CO)H$_2$-M$_{56}$ with respect to the dissociative loss of H$_2$. This is a particularly interesting result, as the original H$_2$/D$_2$ dissociative exchange reaction reported by Shapley and co-workers[4] has recently been suggested to proceed through the cationic trihydride, possibly catalyzed by adventitious acid.[2] To establish which of these processes actually operates for intrazeolite CpIr(CO)H$_2$-M$_{56}$Y will require much more work, especially as a "fully" alkali-metal exchange zeolite Y sample always contains "trace" amounts of Brønsted acid sites.

(c) Alkanes and Arenes. Another point that deserves mentioning concerns **our numerous failed attempts** to produce intrazeolite C–H bond activation products of the type CpIr(CO)(R)H-M$_{56}$Y with thermal and photolytic treatments of CpIr(CO)H$_2$-M$_{56}$Y with methane, pentane, and benzene. The ν_{CH}, ν_{IrH}, and ν_{CO} modes of the CpIr(CO)H$_2$-M$_{56}$Y species remain unaltered throughout these processes, leading one to the surprising conclusion that, in contrast to the situation in solution and cryogenic matrices,[5] the intrazeolite system is unable to participate in C–H bond insertion chemistry involving alkanes and arenes.

(d) Brønsted Acid and Proton-Loaded Zeolite Y. The intrazeolite reactions of CpIr(CO)H$_2$ with Brønsted acid sites generated

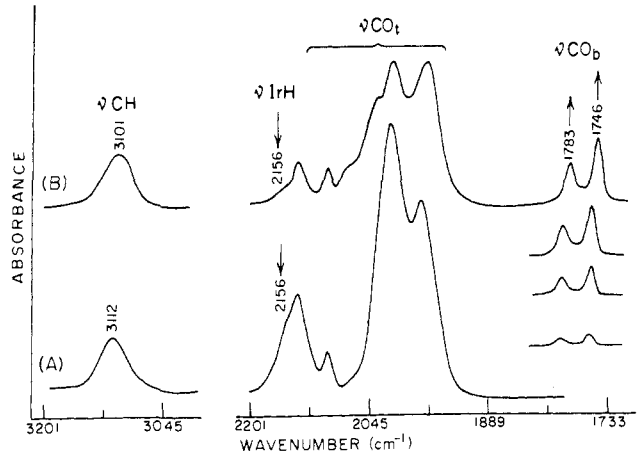

Figure 6. Mid-IR spectrum of (A) freshly impregnated $CpIr(CO)H_2$–$H_{56}Y$ and (B) the same sample on standing at room temperature and recorded at various times up to 24 h.

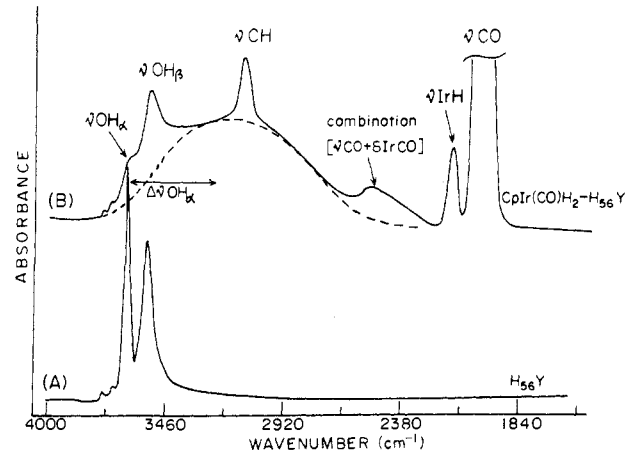

Figure 7. Mid-IR spectra of (A) $H_{56}Y$ and (B) freshly impregnated $CpIr(CO)H_2$–$H_{56}Y$.

from thermal vacuum deamination of $(NH_4)_{56}Y \rightarrow H_{56}Y$ and with acid sites generated from the adsorption of anhydrous HX into $M_{56}Y$, namely, proton-loaded $(HX)_n$–$M_{56}Y$,[27] both proved to be very interesting. Recall that solution-phase protonation of $CpIr(CO)H_2$ has not yet been reported. By contrast, Heinekey and Payne[7] have proposed that protonation of $CpIrLH_2$ (where L = PPh_3, PMe_3, and $AsPh_3$) by $HBF_4 \cdot Et_2O$ produces the amazing trihydrogen species $CpIrL(H_3)^+$.

When $CpIr(CO)H_2$ is impregnated into dehydrated, fully exchanged acid zeolite Y $H_{56}Y$, one immediately observes a complex series of new ν_{CO} modes between 2100 and 1900 cm^{-1} coexisting with the ν_{CH}, ν_{IrH}, and ν_{CO} bands of some remaining quantity of the original $CpIr(CO)H_2$–$M_{56}Y$ (Figure 6). From this point on, one observes **only** the slow decay of the diagnostic bands of the latter species, with concomitant growth of a pair of well-resolved bands in the carbonyl-bridging region at 1783 and 1746 cm^{-1} and an accompanying ν_{CH} mode of coordinated Cp at 3101 cm^{-1} (Figure 6). The group of new bands in the range 2100–1900 cm^{-1} remains invariant throughout this process. By comparison with the experiments of Gil, Haddleton, and Ozin,[8] in which $CpIr(CO)_2$ is encapsulated in $H_{56}Y$, one realizes that the 2100–1900–cm^{-1} collection of ν_{CO} modes is exactly common to the two systems. These have been established to be associated with a mixture of $CpIr(CO)_2H^+$ and $CpIr(CO)_2$ housed in the supercage of $H_{56}Y$.[8]

It is worth noting that, at saturation loading levels of about 16 $CpIr(CO)H_2$–$H_{56}Y$, one observes essentially complete annihilation of the α-cage Brønsted acid sites (Figure 7), thereby providing compelling evidence that, under these conditions, the

(27) Ozin, G. A.; Özkar, S.; McMurray, L. *J. Phys. Chem.* **1990**, *94*, 8289, 8297. Ozin, G. A.; Özkar, S.; Stucky, G. *J. Phys. Chem.* **1990**, *94*, 7562.

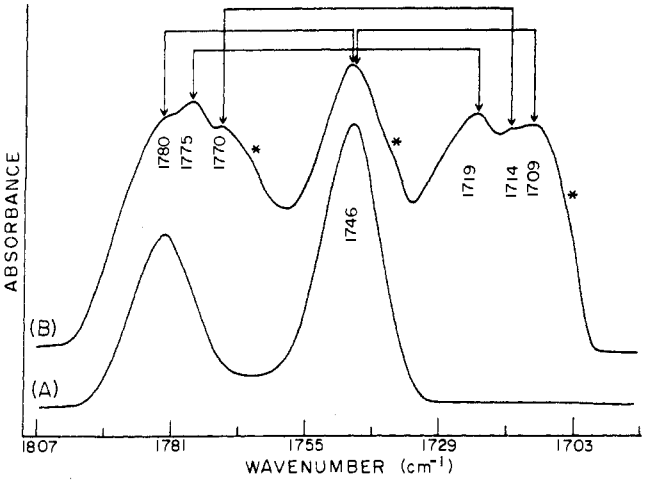

Figure 8. Mid-IR spectra in the ν_{CO} region of (A) $Cp_2Ir_2(^{12}CO)_2$–$H_{56}Y$ and (B) $Cp_2Ir_2(^{12}CO)_n(^{13}CO)_{2-n}$–$H_{56}Y$, the former and the latter being generated from the proton-induced, reductive-elimination, dimerization reaction of $CpIr(^{12}CO)H_2$–$H_{56}Y$ and a 1:1 mixture of $CpIr(^{12}CO)H_2$/$CpIr(^{13}CO)H_2$–$H_{56}Y$, respectively. Secondary anchoring site effects indicated by an asterisk.

Scheme III

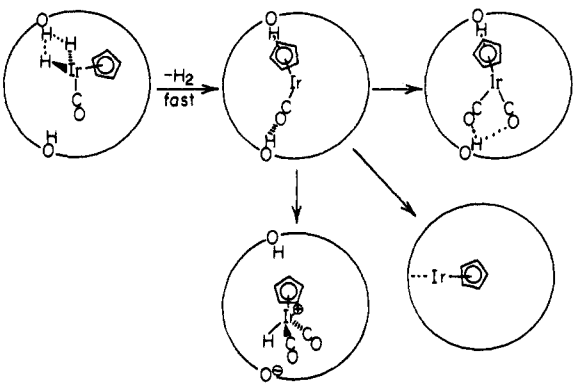

Scheme IV

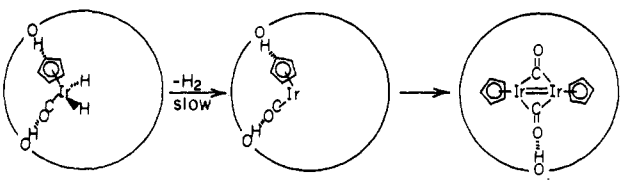

$CpIr(CO)H_2$ precursor is homogeneously distributed throughout the α-cage void volume of $H_{56}Y$.

From consideration of the above results, it is believed that there are at least **two** independent reactions of the $CpIr(CO)H_2$ complex with the acid sites of $H_{56}Y$. The first one is considered to be a fast proton-induced, reductive-elimination, disproportionation reaction of the type illustrated in Scheme III that occurs immediately upon impregnation of $CpIr(CO)H_2$ into $H_{56}Y$. The second reaction is a much slower one in which over a period of about 24 h a carbonyl-bridged dimer species is formed by a process probably involving a $CpIr(CO)H_2$–$H_{56}Y$ anchoring site, which is less susceptible to dissociative loss of H_2 as illustrated in Scheme IV. The proposed $Cp_2Ir_2(CO)_2$–$H_{56}Y$ bridged dimer species is so far unknown in the solution/solid-phase chemistry of Ir(I). In fact, the decarbonylation product of $CpIr(CO)H_2$ in solution is the $Cp_3Ir_3(CO)_3$ trimer species[3] (Scheme I). It may be the size constraints imposed by the α-cage, the low concentration of $CpIr(CO)H_2$, or proton-stabilizing interactions with the dimer that prohibit the formation of trimer from the proposed 16e intrazeolite reaction intermediate $CpIr(CO)\cdots H_{56}Y$.

There are various sources of experimental data that lead one to believe that the observed bands in the ν_{CH} and ν_{CO} regions for

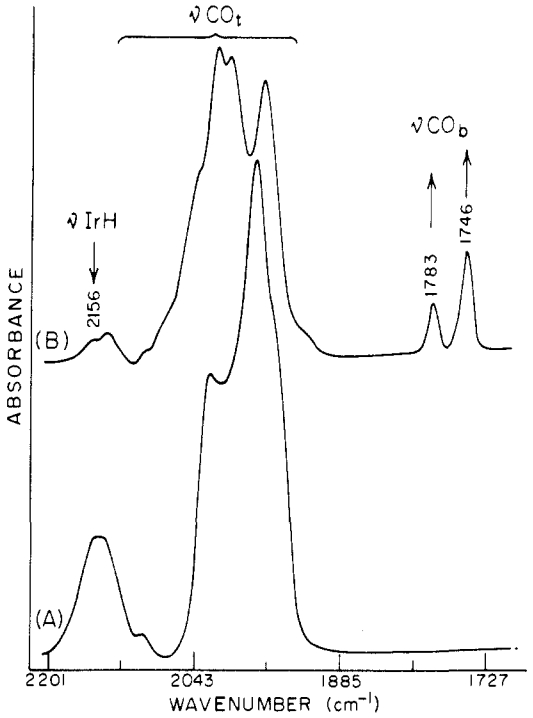

Figure 9. Mid-IR spectra of (A) freshly impregnated $CpIr(CO)H_2$–$(HBr)_8$–$Na_{56}Y$ and (B) the same sample on standing at room temperature for 24 h.

this reaction product are indeed those of the encapsulated dimer, which is in fact bonding asymmetrically via a single carbonyl of the bridge to a single Brønsted acid site. These are laid out below.

(i) $CpIr(CO)D_2$–$H_{56}Y$ yields the identical dimer product spectrum.

(ii) $CpIr(CO)H_2$–$D_{56}Y$ yields the identical dimer product spectrum with no evidence for H/D scrambling.

(iii) A 1:1 mixture of $CpIr(^{12}CO)H_2/CpIr(^{13}CO)H_2$–$H_{56}Y$ yields **seven** clearly observable bridge ν_{CO} bands (Figure 8) in place of the original **two** (Figure 6).

(iv) Identical results are obtained with proton-loaded zeolite Y $(HX)_8$–$Na_{56}Y$ (where X = Cl and Br) (Figure 9).

(v) H_2 impedes the formation of dimer product.

(vi) The dimer reacts with CO at room temperature to yield the known species $CpIr(CO)_2$–$M_{56}Y$ anchored within the supercage in sites identical with those found by direct impregnation of $CpIr(CO)_2$ into $M_{56}Y$.[8]

(vii) The dimer does not react with H_2 or D_2.

(viii) The known carbonyl-bridged dimer $Cp_2Co_2(CO)_2$–$M_{56}Y$ has a ν_{CH} and ν_{CO} mid-IR spectrum very similar to that of the iridium dimer product.[8b]

It is apparent from the above information that the 1783/1746-cm^{-1} doublet (Figure 6) is **not** hydridic in nature (no observed D-shift) and is instead unequivocally of bridging ν_{CO} character (Figure 8). The absence of the dimerization reaction for $CpIr(CO)H_2$–$M_{56}Y$ (M = Li, Na, K, Rb, Cs) implicates protons as the activating groups; however, the product does not seem to bear any Ir–H bonds. The "triggering action" induced by protons is confirmed by the observation of the same dimerization reaction with proton-loaded zeolite Y, namely, $CpIr(CO)H_2$–$(HX)_8$–$Na_{56}Y$ (Figure 9). (Note that, in $(HX)_8$–$Na_{56}Y$, the HX has been recently shown to exist as the charge-separated species $ZONa^+X^-$ and ZOH, where the former moiety is best described as a tight cation–anion pair, while the latter species behaves as a "normal" Brønsted acid site.[27] The loading of HX was chosen such that HX is not present in sufficient quantities to produce solvated protons $(ZOH\cdots(X\text{–}H)_n)$.[27]

The dicarbonyl stoichiometry for the proposed $Cp_2Ir_2(CO)_2$–$H_{56}Y$ dimer species receives some support from the results of a $^{12}CO/^{13}CO$ mixed isotopic labeling study with a 1:1 mixture of labeled precursors $CpIr(^{12}CO)H_2/CpIr(^{13}CO)H_2$–$H_{56}Y$ (Figure 8). In these experiments, the original two $\nu_{^{12}CO}$ bridge modes at 1783 and 1746 cm^{-1} (Figure 6) yield **seven** main bands around 1783, 1775, 1770, 1746, 1719, 1714, and 1709 cm^{-1} with some evidence for secondary anchoring site effects (weak shoulders indicated with an asterisk in Figure 8). Had the species been a **centrosymmetrical** dicarbonyl containing **equivalent** bridging CO ligands, a maximum of **six** IR-active ν_{CO} modes arising from **three** unique isotopomers would be observable in a $^{12}CO/^{13}CO$ mixed-isotope experiment, namely, $Cp_2Ir_2(^{12}CO)_n(^{13}CO)_{2-n}$–$H_{56}Y$ (n = 0–2). On the other hand, if the bridging CO ligands were somehow made to be inequivalent (for example, by asymmetrically hydrogen bonding to a Brønsted acid site as sketched in Scheme IV), then there should exist **eight** IR ν_{CO} modes arising from **four** unique isotopomers in a $Cp_2Ir_2(^{12}CO)_n{}^*(^{13}CO)_{2-n}$–$H_{56}Y$ experiment as laid out in Table I (the asterisks in Table I indicate that one of the two CO ligands is involved in hydrogen bonding to a Brønsted acid site).

Table I. Observed and Calculated Carbonyl Stretching Frequencies (cm^{-1}) for $Cp_2Ir_2(^{12}CO)_n{}^*(^{13}CO)_{2-n}$–$H_{56}Y$ Containing an Asymmetrical Carbonyl Bridge[a]

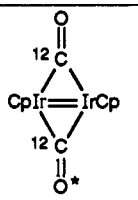 (1)		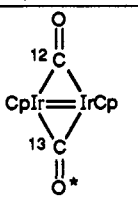 (2)		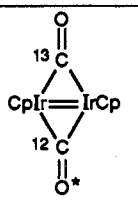 (3)		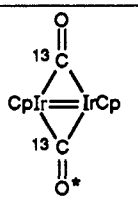 (4)	
obsd	calcd	obsd	calcd	obsd	calcd	obsd	calcd
1783	1784	1775	1773	1770	1772	1746	1745
1746	1746	1719	1718	1714	1718	1709	1707

[a] Best fit Cotton–Kraihanzel force constants: f_r = 12.60; f_r' = 12.55; f_{rr}' = 0.30 mdyn Å^{-1}. RMS error in eigenvalues is 2.2 cm^{-1}.

Using the Cotton–Kraihanzel (C–K) force field approximation[19] for the proposed asymmetrically carbonyl bridge anchored $Cp_2Ir_2(^{12}CO)_n{}^*(^{13}CO)_{2-n}$–$H_{56}Y$ isotopomers (n = 0–2), one finds good agreement between the **seven** observed and **eight** calculated ν_{CO} stretching frequencies as seen by inspection of Figure 8 and Table I. These results provide compelling support for the carbonyl-bridged-dimer proposal. An explanation for the "missing" eighth ν_{CO} mode of the dimer is found in the realization that an accidental overlap of two ν_{CO} bands is expected to occur around 1746 cm^{-1} between the asymmetric ν_{CO} mode of isotopomer **1** and the symmetric ν_{CO} mode of isotopomer **4** (Figure 8, Table I). The computed best fit C–K force constants f_r, $f_r{}^*$, and $f_{rr}{}^*$ that emerge from this calculation are listed in Table I, where the root mean square error in the eigenfrequencies is found to be 2.2 cm^{-1}.

A final point worth discussion concerns the absence of any observable H/D-exchange processes when $CpIr(CO)H_2$ is impregnated into $D_{56}Y$ as described earlier. This implies that, in both the **fast** proton-induced reductive-elimination disporportionation and **slow** dimerization reactions observed for $CpIr(CO)H_2$–$H_{56}Y$, one does not have to consider protonation reactions to species of the types $CpIr(CO)(H_3)^+$, $CpIr(CO)(\eta^2\text{–}H_2)(H)^+$, and $CpIr(CO)(H)_3$. Instead, $CpIr(CO)H_2$–$H_{56}Y$ anchoring modes involving hydrogen-bonding interactions of the type proposed in Schemes III and IV appear to be the major actors participating in the intrazeolite disproportionation–dimerization chemistry observed in Brønsted acid $H_{56}Y$ and proton-loaded $(HX)_8$–$Na_{56}Y$.

It is worth noting that Graham and Heinekey et al.[28] very recently reported the synthesis and crystal structure of $Cp_2{}^*Ir_2(CO)_2$, which is precisely the analogue of our intrazeolite $Cp_2Ir_2(CO)_2$–$H_{56}Y$ system. Recall that Wrighton and Anderson[29] showed that near-UV irradiation of $Cp_2Rh_2(CO)_3$ in low-temperature hydrocarbon matrices results in rapid and clean loss of CO to produce the metal–metal double-bonded doubly CO bridged

(28) Ball, R. G.; Graham, W. A. G.; Heinekey, D. M.; Hoyano, J. K.; McMaster, A. D.; Mattson, B. M.; Michel, S. T. *Inorg. Chem.* **1990**, *29*, 2023.
(29) Anderson, F. R.; Wrighton, M. S. *Inorg. Chem.* **1986**, *25*, 112.

Scheme V

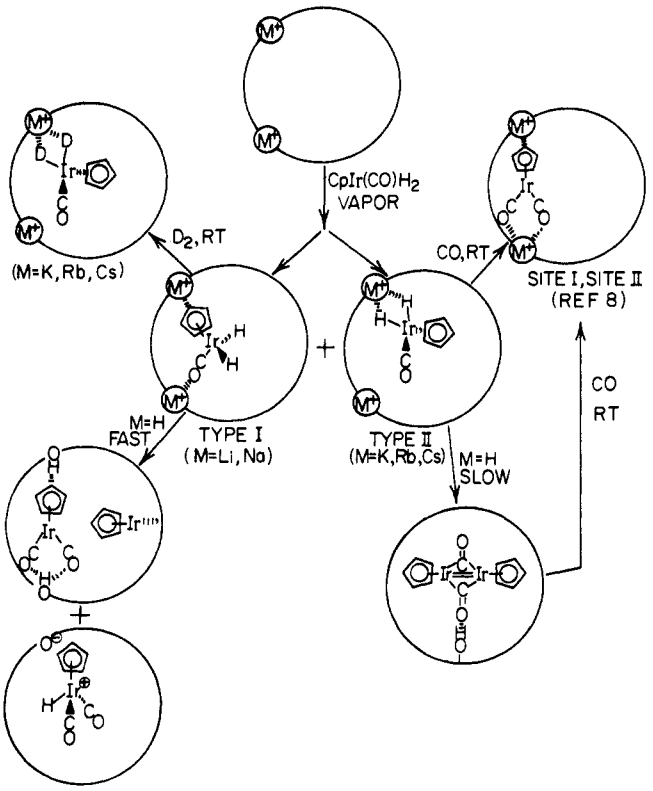

product $Cp_2Rh_2(CO)_2$, while room temperature irradiation of $Cp_2^*Rh_2(CO)_3$ by Herrmann et al.[30] leads to $Cp_2^*Rh_2(CO)_2$.

Summary

The key discoveries to emerge from this first investigation of the impregnation of gaseous $CpIr(CO)H_2$ into alkali-metal cation, Brønsted acid, and proton-loaded forms of dehydrated zeolite Y are collected together in the form of Scheme V. Here one finds that the thermally equilibrated anchoring geometries of $CpIr(CO)H_2$ are of the forms denoted type I and type II. It appears to be the mutual spacial and topological requirements of the organometallic guest and α-cage site II alkali-metal cations that determine whether the binding sites involve primary interactions between $M^+\cdots Cp/M^+\cdots OC$ (M = Li, Na; type I) or $M^+\cdots H$ (M = K, Rb, Cs; type II). The type II species appears to be activated toward room temperature H_2/D_2 exchange reactions without any H/D hydride or Cp ring scrambling, therefore implicating a dissociative pathway for the exchange process. With CO at room temperature, one observes rapid intrazeolite conversion to the known $CpIr(CO)_2$–$M_{56}Y$ species. Surprisingly in contrast to the situation that is found in solution, neither thermal nor photochemical C–H bond activation chemistry to yield $CpIr(CO)(R)H$–$M_{56}Y$ species has yet been observed for $CpIr(CO)H_2$–$M_{56}Y$ in contact with methane, pentane, and benzene. The intrazeolite chemistry of $CpIr(CO)H_2$ in $H_{56}Y$ and in $(HX)_8$–$Na_{56}Y$ acid zeolites does not appear to lead to simple protonation reactions involving species such as $CpIr(CO)(H_3)^+$, $CpIr(CO)(H)(\eta^2\text{-}H_2)^+$, and $CpIr(CO)(H)_3^+$. Instead, one observes two types of novel intrazeolite chemistry: (i) a fast process that operates during the deposition step and appears to be best described as a proton-induced, reductive-elimination, disproportionation reaction to yield anchored $CpIr(CO)_2$, CpIr, and $CpIr(CO)_2H^+$ species, followed by (ii) a much slower process considered to arise from a proton-induced, reductive-elimination, dimerization reaction to yield the novel binuclear species $Cp_2Ir_2(CO)_2$–$H_{56}Y$. The latter is formulated as having a bridged dicarbonyl structure and is therefore the analogue of the recently discovered intrazeolite $Cp_2Co_2(CO)_2$–$M_{56}Y$ species, which by contrast is most effectively generated from a thermally induced carbonyl dissociation–dimerization reaction of $CpCo(CO)_2$–$M_{56}Y$. Mixed $^{12}CO/^{13}CO$ isotope substitution studies show that the $Cp_2Ir_2(CO)_2$–$H_{56}Y$ dimer species is most likely anchored asymmetrically, via one of its bridging carbonyl ligands, through a hydrogen-bonding interaction with an α-cage Brønsted acid site.

Acknowledgment. We acknowledge the Natural Sciences and Engineering Research Council of Canada's Operating and Strategic Grants Programmes and Imperial Oil for generous financial support of this work. S.Ö. expresses his gratitude to the Middle East Technical University for granting him an extended leave of absence to conduct his research at the University of Toronto. Supplies of high-quality zeolites from Dr. Edith Flanigen at Union Carbide, Tarrytown, NY, are gratefully appreciated. We also thank all of our co-workers at Toronto for many stimulating and enlightening discussions during the course of this work.

(30) Plank, J.; Riedle, D.; Herrmann, W. A. *Angew. Chem., Int. Ed. Engl.* **1980**, *19*, 937.